Available online at www.sciencedirect.com
ScienceDirect
International Journal of Plasticity 23 (2007) 207–226
INTERNATIONAL JOURNAL OF Plasticity
www.elsevier.com/locate/ijplas

A three-dimensional model describing stress-induced solid phase transformation with permanent inelasticity

F. Auricchio [a,b,c], A. Reali [a,c,*], U. Stefanelli [b]

[a] *Dipartimento di Meccanica Strutturale, Università degli Studi di Pavia, Via Ferrata 1, 27100 Pavia, Italy*
[b] *Istituto di Matematica Applicata e Tecnologie Informatiche del CNR, Pavia, Italy*
[c] *European School for Advanced Studies in Reduction of Seismic Risk (ROSE School), Università degli Studi di Pavia, Italy*

Received 25 September 2005
Available online 1 September 2006

Abstract

The employment of shape memory alloys (SMA) in a large number of applications in the fields of aeronautical, biomedical, and structural engineering has been the motivation for an increasing interest in the direction of a correct and exhaustive modeling of their macroscopic behaviour.

Many models for SMA available in the literature consider fully reversible phase transformations (i.e. no permanent inelastic strains), which are proved by experiments to be sometimes a not fully realistic approximation. In this paper we propose a new three-dimensional model which is capable of including permanent inelastic effects combined with a good description of pseudo-elastic and shape-memory behaviours. Moreover, we report the numerical results from a number of both uniaxial and non-proportional biaxial tests, which aim at assessing model features and performance.

Keywords: Shape memory alloys; Permanent inelasticity; Phase transformation; Pseudo-elasticity; Shape-memory effect; Non-proportional biaxial tests

* Corresponding author. Address: Dipartimento di Meccanica Strutturale, Università degli Studi di Pavia, Via Ferrata 1, 27100 Pavia, Italy. Tel.: +39 0382 985475; fax: +39 0382 528422.
E-mail address: alessandro.reali@unipv.it (A. Reali).

0749-6419/$ - see front matter
doi:10.1016/j.ijplas.2006.02.012

1. Introduction

The great and always increasing interest in SMA materials (cf. Duerig et al., 1990; Duerig and Pelton, 2003) and their industrial applications in many branches of engineering is deeply stimulating the research on constitutive laws. As a consequence, many models able to reproduce one or both of the well-known SMA macroscopic behaviours, referred to as *pseudo-elasticity* and *shape-memory effect*, have been proposed in the literature in the last years (refer for instance to Bouvet et al., 2004; Govindjee and Miehe, 2001; Helm and Haupt, 2003; Leclercq and Lexcellent, 1996; Levitas, 1998; Levitas and Preston, 2002a,b; Peultier et al., 2004; Raniecki and Lexcellent, 1994).

In particular, the constitutive law proposed by Souza et al. (1998) and improved by Auricchio and Petrini (2004a) seems to be attractive. Developed within the theory of irreversible thermodynamics, this model is in fact able to describe both pseudo-elasticity and shape-memory effect and the corresponding solution algorithm is simple and robust as it is based on a plasticity-like return map procedure.

Moreover, we have to stress that most of the SMA models present in the literature are not able to reproduce other experimentally observed SMA behaviours such as permanent inelasticity and degradation effects. As an example, Fig. 1 (Arrigoni et al., 2001) reports the experimental stress–strain response of a Ni–Ti wire subjected to a strain driven uniaxial cyclic tension test up to 6% strain. It is remarkable that pseudo-elastic loops show an increasing level of permanent inelasticity that saturates on a stable value after a certain number of cycles. The same figure highlights that degradation effects should be taken into account as well. For a description of these behaviours from a physical point of view the interested reader is referred to classical SMA textbooks such as Funakubo (1987) and Otsuka and Wayman (1998). We remark that permanent inelasticity is present not only in Ni–Ti alloys, but also in other kinds of SMA (cf., e.g., Dutkiewicz, 1994; Šittner et al., 1995; Vandermeer et al., 1981). Moving from these experimental evidences, some models accounting for permanent inelastic effects have been recently proposed in the

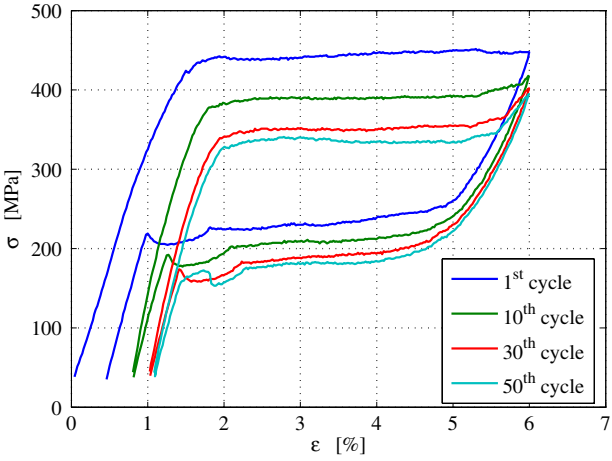

Fig. 1. Experimental results on a SMA Ni–Ti wire. Cyclic tension test: stress versus strain up to 6% strain.

literature (see, e.g., Bo and Lagoudas, 1999; Govindjee and Kasper, 1997; Lagoudas and Entchev, 2004; Paiva et al., 2005).

Taking its basis in this framework, the present paper addresses a new three-dimensional phenomenological constitutive model able to reproduce pseudo-elastic and shape-memory behaviours as well as to include permanent inelasticity and degradation effects. The model consists of an extension of the model discussed by Souza et al. (1998) and Auricchio and Petrini (2004a), by means of the introduction of a new internal variable describing permanent inelastic strains. In this work, an analytic description of the constitutive equations is presented together with numerical experiments which show main features and performance of the model.

We finally remark that a 1D version of the proposed model has been recently presented by Auricchio and Reali (2005).

2. 3D phenomenological model for stress-induced solid phase transformation with permanent inelasticity

2.1. Time-continuous frame

The model assumes the total strain $\boldsymbol{\varepsilon}$ and the absolute temperature T as control variables, the transformation strain $\boldsymbol{e}^{\mathrm{tr}}$ and the permanent inelastic strain $\boldsymbol{q}$ as internal ones. As in Auricchio and Petrini (2004a), the second-order tensor $\boldsymbol{e}^{\mathrm{tr}}$ describes the strain associated to the transformation between the two solid phases referred to as martensite and austenite. Here, this quantity has no fully reversible evolution and the permanent inelastic strain $\boldsymbol{q}$ gives a measure of the part of $\boldsymbol{e}^{\mathrm{tr}}$ that cannot be recovered when unloading to a zero stress state. Moreover, we require that

$$\|\boldsymbol{e}^{\mathrm{tr}}\| \leqslant \varepsilon_L, \tag{1}$$

where $\|\cdot\|$ is the usual Euclidean norm and ε_L is a material parameter corresponding to the maximum transformation strain reached at the end of the transformation during an uniaxial test.

Assuming a small strain regime, justified by the fact that the approximation of large displacements and small strains is valid for several applications, the following standard additive decomposition can be considered

$$\boldsymbol{\varepsilon} = \frac{\theta}{3}\mathbf{1} + \boldsymbol{e},$$

where $\theta = \mathrm{tr}(\boldsymbol{\varepsilon})$ and $\boldsymbol{e}$ are, respectively, the volumetric and the deviatoric part of the total strain $\boldsymbol{\varepsilon}$, while $\mathbf{1}$ is the second-order identity tensor. The free energy density function Ψ for a polycrystalline SMA material is then expressed as the convex potential

$$\begin{aligned}\Psi(\theta, \boldsymbol{e}, T, \boldsymbol{e}^{\mathrm{tr}}, \boldsymbol{q}) = {} & \frac{1}{2}K\theta^2 + G\|\boldsymbol{e} - \boldsymbol{e}^{\mathrm{tr}}\|^2 + \beta\langle T - M_{\mathrm{f}}\rangle\|\boldsymbol{e}^{\mathrm{tr}} - \boldsymbol{q}\| + \frac{1}{2}h\|\boldsymbol{e}^{\mathrm{tr}}\|^2 \\ & + \frac{1}{2}H\|\boldsymbol{q}\|^2 - A\boldsymbol{e}^{\mathrm{tr}} : \boldsymbol{q} + \mathscr{I}_{\varepsilon_L}(\boldsymbol{e}^{\mathrm{tr}}),\end{aligned} \tag{2}$$

where K and G are, respectively, the bulk and the shear modulus, β is a material parameter related to the dependence of the critical stress on the temperature, M_{f} is the temperature below which only martensite phase is stable, h defines the hardening of the phase

transformation, H controls the saturation of the permanent inelastic strain evolution, and A controls the degradation of the model. Moreover, we make use of the indicator function

$$\mathscr{I}_{\varepsilon_L}(\boldsymbol{e}^{\mathrm{tr}}) = \begin{cases} 0 & \text{if } \|\boldsymbol{e}^{\mathrm{tr}}\| < \varepsilon_L, \\ +\infty & \text{otherwise} \end{cases}$$

in order to satisfy the transformation strain constraint (1); we also introduce the positive part function $\langle\cdot\rangle$, defined as

$$\langle a \rangle = \begin{cases} a & \text{if } a > 0, \\ 0 & \text{otherwise.} \end{cases}$$

We remark that in the expression of the free energy we neglect the contributions due to thermal expansion and change in temperature with respect to the reference state, since we are not interested here in a complete description of the thermomechanical coupled problem. However, the interested reader may refer to Auricchio and Petrini (2004a,b) to see how it is possible to take into account these aspects in the formulation. We also stress that, due to the fact that we do not consider a fully thermomechanical coupled model, Ψ should be more properly referred to as a temperature-parameterized free energy density function.

Moreover, since we use only a single internal variable second-order tensor to describe phase transformations, at most it is possible to distinguish between a generic parent phase (not associated to any macroscopic strain) and a generic product phase (associated to a macroscopic strain), as in Auricchio and Petrini (2004a). Accordingly, the model does not distinguish between the austenite and the twinned martensite, as both these phases do not produce macroscopic strain.

We furthermore highlight that, for the sake of simplicity, the present model does not reflect the difference existing between the austenite and the martensite elastic properties.

Starting from the free energy function Ψ and following standard arguments, we can derive the constitutive equations

$$\begin{aligned}
p &= \frac{\partial \Psi}{\partial \theta} = K\theta, \\
\boldsymbol{s} &= \frac{\partial \Psi}{\partial \boldsymbol{e}} = 2G(\boldsymbol{e} - \boldsymbol{e}^{\mathrm{tr}}), \\
\eta &= -\frac{\partial \Psi}{\partial T} = -\beta \|\boldsymbol{e}^{\mathrm{tr}} - \boldsymbol{q}\| \frac{\langle T - M_{\mathrm{f}} \rangle}{|T - M_{\mathrm{f}}|}, \\
\boldsymbol{X} &= -\frac{\partial \Psi}{\partial \boldsymbol{e}^{\mathrm{tr}}} = \boldsymbol{s} - \beta \langle T - M_{\mathrm{f}} \rangle \frac{\boldsymbol{e}^{\mathrm{tr}} - \boldsymbol{q}}{\|\boldsymbol{e}^{\mathrm{tr}} - \boldsymbol{q}\|} - h\boldsymbol{e}^{\mathrm{tr}} + A\boldsymbol{q} - \gamma \frac{\boldsymbol{e}^{\mathrm{tr}}}{\|\boldsymbol{e}^{\mathrm{tr}}\|}, \\
\boldsymbol{Q} &= -\frac{\partial \Psi}{\partial \boldsymbol{q}} = \beta \langle T - M_{\mathrm{f}} \rangle \frac{\boldsymbol{e}^{\mathrm{tr}} - \boldsymbol{q}}{\|\boldsymbol{e}^{\mathrm{tr}} - \boldsymbol{q}\|} - H\boldsymbol{q} + A\boldsymbol{e}^{\mathrm{tr}},
\end{aligned} \tag{3}$$

where $p = \mathrm{tr}(\boldsymbol{\sigma})/3$ and $\boldsymbol{s}$ are, respectively, the volumetric and the deviatoric part of the stress $\boldsymbol{\sigma}$, $\boldsymbol{X}$ is a thermodynamic stress-like quantity associated to the transformation strain $\boldsymbol{e}^{\mathrm{tr}}$, $\boldsymbol{Q}$ is a thermodynamic stress-like quantity associated to the permanent inelastic strain $\boldsymbol{q}$, and η is the entropy. The variable γ results from the indicator function subdifferential $\partial \mathscr{I}_{\varepsilon_L}(\boldsymbol{e}^{\mathrm{tr}})$ and it is defined as

$$\begin{cases} \gamma = 0 & \text{if } \|\boldsymbol{e}^{\mathrm{tr}}\| < \varepsilon_L, \\ \gamma \geqslant 0 & \text{if } \|\boldsymbol{e}^{\mathrm{tr}}\| = \varepsilon_L, \end{cases}$$

so that $\partial \mathscr{I}_{\varepsilon_L}(\boldsymbol{e}^{\mathrm{tr}}) = \gamma \frac{\boldsymbol{e}^{\mathrm{tr}}}{\|\boldsymbol{e}^{\mathrm{tr}}\|}$.

To describe phase transformation and inelasticity evolution, we choose (following a plasticity-like terminology) a limit function F defined as

$$F(\boldsymbol{X}, \boldsymbol{Q}) = \|\boldsymbol{X}\| + \kappa \|\boldsymbol{Q}\| - R, \tag{4}$$

where κ is a material parameter defining a scaling modulus between the inelastic effect and the phase transformation, while R is the radius of the elastic domain. We stress that, in order to reproduce the asymmetric behaviour in tension and compression shown by SMA in many experiments, different and more complicate choices for F should be introduced in (4), as it is done in Auricchio and Petrini (2004a) where a Prager–Lode type limit function is employed; further inspiration can be taken also from plasticity literature, where interesting anisotropic limit functions have been recently proposed (see, e.g., Barlat et al., 2005; Yeh and Lin, 2006). However, this issue is beyond the purpose of the present paper and such an enhancement will be addressed in a forthcoming contribution.

Considering an associative framework, the flow rules for the internal variables take the form

$$\begin{aligned} \dot{\boldsymbol{e}}^{\mathrm{tr}} &= \dot{\zeta} \frac{\partial F}{\partial \boldsymbol{X}} = \dot{\zeta} \frac{\boldsymbol{X}}{\|\boldsymbol{X}\|}, \\ \dot{\boldsymbol{q}} &= \dot{\zeta} \frac{\partial F}{\partial \boldsymbol{Q}} = \dot{\zeta} \kappa \frac{\boldsymbol{Q}}{\|\boldsymbol{Q}\|}. \end{aligned} \tag{5}$$

The model is finally completed by the classical Kuhn–Tucker conditions

$$\begin{aligned} &\dot{\zeta} \geqslant 0, \\ &F \leqslant 0, \\ &\dot{\zeta} F = 0. \end{aligned} \tag{6}$$

Observation 1. By exploiting basic Convex Analysis tools (see, e.g., Clarke, 1990) we can rewrite our constitutive model (3)–(6) in the equivalent form

$$\begin{pmatrix} -p \\ -\boldsymbol{s} \\ \eta \\ \partial D \begin{pmatrix} \dot{\boldsymbol{e}}^{\mathrm{tr}} \\ \dot{\boldsymbol{q}} \end{pmatrix} \end{pmatrix} + \partial \Psi \begin{pmatrix} \theta \\ \boldsymbol{e} \\ T \\ \boldsymbol{e}^{\mathrm{tr}} \\ \boldsymbol{q} \end{pmatrix} \ni \boldsymbol{0}. \tag{7}$$

Here ∂D stands for the subdifferential of the function D defined as

$$D(\boldsymbol{e}^{\mathrm{tr}}, \boldsymbol{q}) = \sup_{F(\boldsymbol{A}, \boldsymbol{B}) \leqslant 0} \{\boldsymbol{A} : \boldsymbol{e}^{\mathrm{tr}} + \boldsymbol{B} : \boldsymbol{q}\}, \tag{8}$$

which is the dissipation function associated to the phase transformation mechanism. It can be shown that

$$D(\boldsymbol{e}^{\mathrm{tr}},\boldsymbol{q}) = \begin{cases} \max\left\{\dfrac{R||\boldsymbol{q}||}{\kappa}, R||\boldsymbol{e}^{\mathrm{tr}}||\right\} & \text{if } \kappa \neq 0, \\ R||\boldsymbol{e}^{\mathrm{tr}}|| & \text{if } \kappa = 0 \text{ and } ||\boldsymbol{q}|| = 0, \\ +\infty & \text{if } \kappa = 0 \text{ and } ||\boldsymbol{q}|| \neq 0, \end{cases}$$

as well as that D is the Fenchel–Legendre conjugate of the indicator function of the non-empty, convex, and closed domain

$$\mathscr{E} = \{(\boldsymbol{A},\boldsymbol{B}) : F(\boldsymbol{A},\boldsymbol{B}) \leqslant 0\}.$$

Hence, it is easy to check that D is positively 1-homogeneous, that is

$$D(\lambda(\boldsymbol{e}^{\mathrm{tr}},\boldsymbol{q})) = \lambda D(\boldsymbol{e}^{\mathrm{tr}},\boldsymbol{q}) \quad \forall \lambda > 0.$$

Namely, the time-evolution of $(\boldsymbol{e}^{\mathrm{tr}},\boldsymbol{q})$ is of rate-independent type since we readily have that

$$\partial D(\lambda(\boldsymbol{e}^{\mathrm{tr}},\boldsymbol{q})) = \partial D(\boldsymbol{e}^{\mathrm{tr}},\boldsymbol{q}) \quad \forall \lambda > 0.$$

The formulation of rate-independent evolution problems in terms of a doubly-nonlinear differential inclusion as in (7) has recently attracted a good deal of attention. In particular, the mathematical treatment of relations as (7) is nowadays fairly settled and existence, uniqueness, and time-discretization results are available. The interested reader is referred to the recent survey by Mielke (in press) where a comprehensive collection of mathematical results on doubly-nonlinear rate-independent problems is provided.

Observation 2. The proposed model is thermodynamically consistent. In the current temperature-parameterized situation, we are classically asked to check for the mechanical dissipation inequality

$$\dot{\psi} - \boldsymbol{s} : \dot{\boldsymbol{e}} - p\dot{\theta} \leqslant 0,$$

at least for sufficiently smooth evolutions. Taking (7) into account and owing to standard Convex Analysis results (Brezis, 1973, Lemme 3.3, p. 73), we readily compute that

$$\dot{\psi} - \boldsymbol{s} : \dot{\boldsymbol{e}} - p\dot{\theta} = -(\boldsymbol{X},\boldsymbol{Q}) \cdot (\dot{\boldsymbol{e}}^{\mathrm{tr}},\dot{\boldsymbol{q}}) \geqslant D(\dot{\boldsymbol{e}}^{\mathrm{tr}},\dot{\boldsymbol{q}}) \geqslant 0,$$

and the assertion follows.

The latter computation is performed by assuming the temperature to be constant along the evolution. It is beyond the purposes of this paper to assess the full thermomechanical evolution problem. Let us however stress that, by suitably augmenting the temperature-parameterized strain energy density by a purely caloric contribution (for instance of the form $-c_{\mathrm{s}} T \ln T$ with c_{s} being the specific heat density) and coupling (7) with the energy balance relation, we would be in the position of formulating a full thermomechanical evolution model which can be proved to be consistent with the Second Principle of Thermodynamics in the form of the Clausis–Duhem inequality. We shall address this perspective elsewhere.

Observation 3. We highlight that the choice $\kappa = 0$ leads to recover the model without permanent inelasticity discussed by Auricchio and Petrini (2004a). In fact, setting $\kappa = 0$ in $(5)_2$, we get $\dot{\boldsymbol{q}} = \boldsymbol{0}$, which means that $\boldsymbol{q}$ does not evolve and is always equal to its initial value, i.e. $\boldsymbol{q} \equiv \boldsymbol{0}$.

Observation 4. We start by introducing here some considerations on the model presented by Auricchio and Petrini (2004a), which aim at explaining its capability to undergo fully reversible phase transformations. Such considerations are basilar in order to understand the key idea we have followed to construct the new model introduced in this section.

We focus on the case $\beta\langle T - M_f\rangle > R$, which is indeed the most interesting, and for simplicity we start considering scalar quantities instead of second-order tensors. This is equivalent to study a proportional loading process (i.e. developed along a fixed direction) so that the scalars X, s, and e^{tr} assume the physical meaning of norms for the corresponding tensor-valued quantities. Then, we suppose to be in the condition $F = 0$, that is (recall that $\kappa = 0$)

$$|X| = \left| s - \beta\langle T - M_f\rangle \frac{e^{tr}}{|e^{tr}|} - h e^{tr} \right| = R, \tag{9}$$

which implies

$$s = \beta\langle T - M_f\rangle \frac{e^{tr}}{|e^{tr}|} + h e^{tr} \pm R. \tag{10}$$

Fig. 2 reports the graphical representations of the relation $s = s(e^{tr})$ obtained from expression (10) for the two cases of unloading from compression and unloading from tension, respectively. The figure shows that for each case there exists an interval for s inside which $e^{tr} = 0$. Considering the intersection of the intervals for the two cases, it is possible to conclude that

$$s \in [-\beta\langle T - M_f\rangle + R, \beta\langle T - M_f\rangle - R] \Rightarrow e^{tr} = 0, \tag{11}$$

i.e., if s belongs to the interval $[-\beta\langle T - M_f\rangle + R, \beta\langle T - M_f\rangle - R]$, e^{tr} is necessarily equal to zero. Accordingly, this implies that, due to the continuity of the considered functions, if we are coming from a state with s outside the indicated interval and we are unloading, e^{tr} necessarily approaches zero as s approaches the extreme of such an interval.

Indeed, the very same conclusion holds also in a 3D framework. Still referring to the unloading situation, one can prove that, whenever $\|\boldsymbol{s}\|$ approaches $\beta\langle T - M_f\rangle - R$ and $\boldsymbol{e}^{tr}$ is such that

$$\|\boldsymbol{X}\| = \left\| \boldsymbol{s} - \beta\langle T - M_f\rangle \frac{\boldsymbol{e}^{tr}}{\|\boldsymbol{e}^{tr}\|} - h\boldsymbol{e}^{tr} \right\| = R,$$

then $\|\boldsymbol{e}^{tr}\|$ tends to zero. A proof follows.

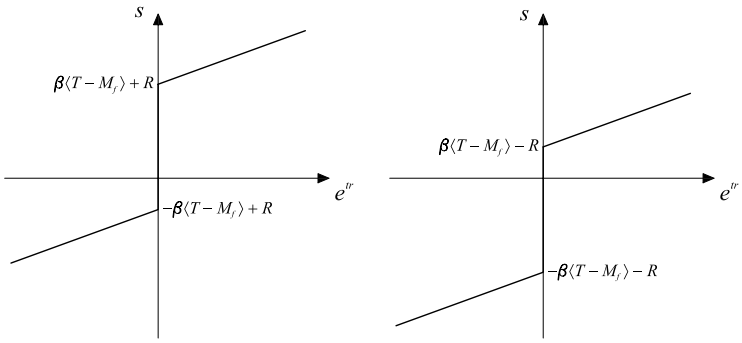

Fig. 2. Plots of $s = s(e^{tr})$ in the cases of unloading from compression (left) and from tension (right).

Assume that this is not the case. Hence, there exists $\varepsilon > 0$ such that, for all $\alpha > 0$, there exist $\boldsymbol{s}_\alpha$, $\boldsymbol{e}^{\mathrm{tr}}_\alpha$ such that

$$\|\boldsymbol{s}_\alpha\| - \beta\langle T - M_{\mathrm{f}}\rangle + R < \alpha,$$
$$\left\|\boldsymbol{s}_\alpha - \beta\langle T - M_{\mathrm{f}}\rangle \frac{\boldsymbol{e}^{\mathrm{tr}}_\alpha}{\|\boldsymbol{e}^{\mathrm{tr}}_\alpha\|} - h\boldsymbol{e}^{\mathrm{tr}}_\alpha\right\| = R,$$

but

$$\|\boldsymbol{e}^{\mathrm{tr}}_\alpha\| > \varepsilon.$$

Then, it suffices to choose $\alpha \leqslant h\varepsilon$ and check that

$$-\|\boldsymbol{s}_\alpha\| > -\beta\langle T - M_{\mathrm{f}}\rangle + R - \alpha,$$
$$\left\|\beta\langle T - M_{\mathrm{f}}\rangle \frac{\boldsymbol{e}^{\mathrm{tr}}_\alpha}{\|\boldsymbol{e}^{\mathrm{tr}}_{\alpha_*}\|} + h\boldsymbol{e}^{\mathrm{tr}}_\alpha\right\| > \beta\langle T - M_{\mathrm{f}}\rangle + h\varepsilon.$$

Now, we take the sum of the latter relations and exploit the Lipschitz continuity of the norm in order to obtain that

$$R < \left\|\beta\langle T - M_{\mathrm{f}}\rangle \frac{\boldsymbol{e}^{\mathrm{tr}}_\alpha}{\|\boldsymbol{e}^{\mathrm{tr}}_\alpha\|} + h\boldsymbol{e}^{\mathrm{tr}}_\alpha\right\| - \|\boldsymbol{s}_\alpha\| \leqslant \left\|\boldsymbol{s}_\alpha - \beta\langle T - M_{\mathrm{f}}\rangle \frac{\boldsymbol{e}^{\mathrm{tr}}_\alpha}{\|\boldsymbol{e}^{\mathrm{tr}}_\alpha\|} - h\boldsymbol{e}^{\mathrm{tr}}_\alpha\right\| = R,$$

which is clearly a contradiction and proves the correctness of our thesis.

Observation 5. We now show the basic idea behind the new model proposed in this paper, arising from the above considerations.

Still referring to the 1D case, if we want to avoid a complete shape recovery (i.e. a fully reversible phase transformation), a simple and effective option consists in substituting the term $\beta\langle T - M_{\mathrm{f}}\rangle e^{\mathrm{tr}}/|e^{\mathrm{tr}}|$ with the new one $\beta\langle T - M_{\mathrm{f}}\rangle (e^{\mathrm{tr}} - q)/|e^{\mathrm{tr}} - q|$. This operation results in translating the graphs in Fig. 2 by a quantity q, as depicted in Fig. 3, leading to the following implication

$$s \in [-\beta\langle T - M_{\mathrm{f}}\rangle + R, \beta\langle T - M_{\mathrm{f}}\rangle - R] \Rightarrow e^{\mathrm{tr}} = q. \tag{12}$$

Relation (12) means that, whenever s is approaching the extreme of the interval $[-\beta\langle T - M_{\mathrm{f}}\rangle + R, \beta\langle T - M_{\mathrm{f}}\rangle - R]$, e^{tr} tends to q, i.e., a permanent inelastic effect is introduced.

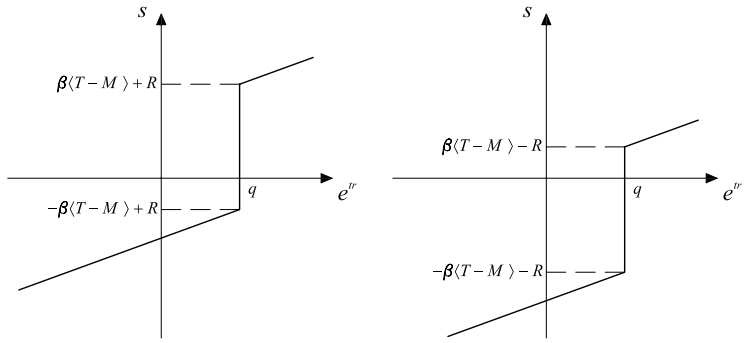

Fig. 3. Translated plots of $s = s(e^{\mathrm{tr}})$ in the cases of unloading from compression (left) and from tension (right).

Analogously, in a 3D setting, substituting the term $\beta\langle T - M_f\rangle \boldsymbol{e}^{tr}/\|\boldsymbol{e}^{tr}\|$ in Eq. (9) with $\beta\langle T - M_f\rangle(\boldsymbol{e}^{tr} - \boldsymbol{q})/\|\boldsymbol{e}^{tr} - \boldsymbol{q}\|$, we obtain that, when unloading, the tensor $\boldsymbol{e}^{tr}$ tends to the permanent inelastic strain tensor $\boldsymbol{q}$.

Observation 6. The parameter κ measures the inelastic effect and its choice is not completely free. For simplicity, we show how to compute an upper bound for this parameter when $h = H = A = 0$ MPa and $\|\boldsymbol{e}^{tr}\| < \varepsilon_L$. Introducing these choices in Eqs. $(3)_4$ and $(3)_5$, the constitutive equations for $\boldsymbol{X}$ and $\boldsymbol{Q}$ take the form

$$\begin{aligned} \boldsymbol{X} &= \boldsymbol{s} - \beta\langle T - M_f\rangle \frac{\boldsymbol{e}^{tr} - \boldsymbol{q}}{\|\boldsymbol{e}^{tr} - \boldsymbol{q}\|}, \\ \boldsymbol{Q} &= \beta\langle T - M_f\rangle \frac{\boldsymbol{e}^{tr} - \boldsymbol{q}}{\|\boldsymbol{e}^{tr} - \boldsymbol{q}\|}. \end{aligned} \tag{13}$$

Now, substituting (13) in the limit function (4) and taking into account the second Kuhn–Tucker condition $(6)_2$, we get

$$F = \|\boldsymbol{X}\| + \kappa\beta\langle T - M_f\rangle - R \leqslant 0.$$

In order to satisfy this inequality, since $\|\boldsymbol{X}\| \geqslant 0$, it is necessary to have

$$\kappa\beta\langle T - M_f\rangle - R \leqslant 0,$$

that leads to the following upper bound for the parameter κ

$$\kappa \leqslant \frac{R}{\beta\langle T - M_f\rangle}.$$

Observation 7. Many experimental studies highlight that SMA show a permanent inelasticity which is not indefinitely evolving but saturates (see for instance Fig. 1). In our model, in the case $T > M_f$, we can introduce such an effect by taking the parameter H different from zero. Considering for computation simplicity the case with $A = 0$ MPa, the constitutive equation for $\boldsymbol{Q}$ simplifies as follows:

$$\boldsymbol{Q} = \beta\langle T - M_f\rangle \frac{\boldsymbol{e}^{tr} - \boldsymbol{q}}{\|\boldsymbol{e}^{tr} - \boldsymbol{q}\|} - H\boldsymbol{q}.$$

Moreover, recalling position $(5)_2$, the evolution of $\boldsymbol{q}$ necessarily stops when $\boldsymbol{Q} = \boldsymbol{0}$, that is when $\boldsymbol{e}^{tr}$ and $\boldsymbol{q}$ are collinear and

$$\|\boldsymbol{q}\| = \frac{\beta\langle T - M_f\rangle}{H}.$$

Hence, whenever the quantities β and M_f and the absolute temperature T are given, we can control the saturation value of $\|\boldsymbol{q}\|$ acting on the material parameter H.

In this way, if we are performing an uniaxial test, we can compute the positive and negative limit values of the scalar q as

$$q^{\pm}_{max} = \pm\sqrt{\frac{2}{3}}\frac{\beta\langle T - M_f\rangle}{H}.$$

We finally highlight that, as proved by the above equations, in the case of stable martensite phase (i.e. $T < M_f$) we cannot obtain an evolution for $\boldsymbol{q}$ unless we take a value of A different from zero.

3. Time-discrete frame

Let us now focus on the crucial issue of computing the stress and internal variable evolution of a SMA sample in a strain-driven situation. We shall directly concentrate ourselves on the solution of the time-incremental problem. Namely, we discretize the time-interval of interest $[0, t_f]$ by means of the partition $I = \{0 = t_0 < t_1 < \cdots < t_{N-1} < t_n = t_f\}$, assume to be given the state of the system $(p_n, \boldsymbol{s}_n, \eta_n, \boldsymbol{e}_n^{tr}, \boldsymbol{q}_n)$ at time t_n, the actual total strain $(\theta, \boldsymbol{e})$ and temperature T at time t_{n+1} (note that for notation simplicity here and in the following we drop the subindex $n+1$ for all the variables computed at time t_{n+1}), and solve for $(p, \boldsymbol{s}, \eta, \boldsymbol{e}^{tr}, \boldsymbol{q})$. For the sake of numerical convenience, instead of solving (3) we prefer to perform some regularization. Indeed, we let $\overline{\|\cdot\|}$ be defined as

$$\overline{\|\boldsymbol{a}\|} = \sqrt{\|\boldsymbol{a}\|^2 + \delta} - \sqrt{\delta},$$

(δ is a user-defined parameter controlling the smoothness of the norm regularization) and introduce the regularized free energy density $\overline{\Psi}$ and limit function $\overline{F}$ as

$$\overline{\Psi}(\theta, \boldsymbol{e}, T, \boldsymbol{e}^{tr}, \boldsymbol{q}) = \frac{1}{2}K\theta^2 + G\|\boldsymbol{e} - \boldsymbol{e}^{tr}\|^2 + \beta\langle T - M_f\rangle\overline{\|\boldsymbol{e}^{tr} - \boldsymbol{q}\|} + \frac{1}{2}h\|\boldsymbol{e}^{tr}\|^2 + \frac{1}{2}H\|\boldsymbol{q}\|^2 - A\boldsymbol{e}^{tr} : \boldsymbol{q} + \mathscr{I}_{\varepsilon_L}(\boldsymbol{e}^{tr}), \tag{14}$$

$$\overline{F}(\boldsymbol{X}, \boldsymbol{Q}) = \|\boldsymbol{X}\| + \kappa\overline{\|\boldsymbol{Q}\|} - R. \tag{15}$$

Finally, the updated values $(p, \boldsymbol{s}, \eta, \boldsymbol{e}^{tr}, \boldsymbol{q})$ for regularized constitutive model can be computed from the following relations:

$$\begin{aligned}
&p = K\theta,\\
&\boldsymbol{s} = 2G(\boldsymbol{e} - \boldsymbol{e}^{tr}),\\
&\eta = -\beta\overline{\|\boldsymbol{e}^{tr} - \boldsymbol{q}\|}\frac{\langle T - M_f\rangle}{|T - M_f|},\\
&\boldsymbol{X} = \boldsymbol{s} - \beta\langle T - M_f\rangle\frac{\boldsymbol{e}^{tr} - \boldsymbol{q}}{\sqrt{\|\boldsymbol{e}^{tr} - \boldsymbol{q}\|^2 + \delta}} - h\boldsymbol{e}^{tr} + A\boldsymbol{q} - \gamma\frac{\boldsymbol{e}^{tr}}{\|\boldsymbol{e}^{tr}\|},\\
&\boldsymbol{Q} = \beta\langle T - M_f\rangle\frac{\boldsymbol{e}^{tr} - \boldsymbol{q}}{\sqrt{\|\boldsymbol{e}^{tr} - \boldsymbol{q}\|^2 + \delta}} - H\boldsymbol{q} + A\boldsymbol{e}^{tr},\\
&\boldsymbol{e}^{tr} = \boldsymbol{e}_n^{tr} + \Delta\zeta\frac{\boldsymbol{X}}{\|\boldsymbol{X}\|},\\
&\boldsymbol{q} = \boldsymbol{q}_n + \Delta\zeta\kappa\frac{\boldsymbol{Q}}{\sqrt{\|\boldsymbol{Q}\|^2 + \delta}},\\
&\overline{F} = \|\boldsymbol{X}\| + \kappa\overline{\|\boldsymbol{Q}\|} - R
\end{aligned} \tag{16}$$

along with the requirements

$$\begin{aligned} &\gamma \geqslant 0, \\ &\|\boldsymbol{e}^{\mathrm{tr}}\| \leqslant \varepsilon_L, \\ &\Delta\zeta \geqslant 0, \quad \overline{F} \leqslant 0, \quad \Delta\zeta\overline{F} = 0, \end{aligned} \tag{17}$$

where $\Delta\zeta = \zeta - \zeta_n = \int_{t_n}^{t_{n+1}} \dot{\zeta}\,\mathrm{d}t$ is the time-integrated consistency parameter.

We shall clearly state that our numerical experiments are not performed on the model of Section 2 but rather on its above-introduced δ-regularized version. This choice turns out to be quite convenient from the numerical viewpoint and preserves most of the characteristic features of the model. Moreover, it can be proved that the δ-regularized model converges to the original one as the regularization parameter δ goes to 0. This fact along with additional mathematical analysis of the model are the subject of the forthcoming contribution Auricchio et al. (in preparation-b); see also Auricchio et al. (in preparation-a) for similar problems.

3.1. Solution algorithm

The solution of the discrete model is performed by means of an elastic-predictor inelastic-corrector return map procedure as in classical plasticity problems (cf. Simo and Hughes, 1998). An elastic trial state is evaluated keeping frozen the internal variables, then a trial value of the limit function is computed to verify the admissibility of the trial state. If this is not verified, the step is inelastic and the evolution equations have to be integrated.

We remark that, as in Auricchio and Petrini (2004a), we distinguish two inelastic phases in our model: a non-saturated phase ($\|\boldsymbol{e}^{\mathrm{tr}}\| < \varepsilon_L$, $\gamma = 0$) and a saturated one ($\|\boldsymbol{e}^{\mathrm{tr}}\| = \varepsilon_L$, $\gamma \geqslant 0$). In our solution procedure we start assuming to be in a non-saturated phase, and when convergence is attained we check if our assumption is violated. If the non-saturated solution is not admissible, we search for a new solution considering saturated conditions.

For each inelastic step, we have to solve the nonlinear system constituted by Eq. (16). As the aim of this paper is to show the model behaviour without focusing on algorithmic problems, we find a solution to the nonlinear system by means of the function *fsolve* implemented in the optimization toolbox of the program MATLAB®.

Observation 8. In the same spirit of Observation 1, we shall now recast the aforementioned algorithm (16) and (17) in terms of dissipation. Exactly as above, we assume to be given the current state of the system $(p_n, \boldsymbol{s}_n, \eta_n, \boldsymbol{e}_n^{\mathrm{tr}}, \boldsymbol{q}_n)$ at time t_n and the actual total strain $(\theta, \boldsymbol{e})$ and temperature T at time t_{n+1}. Then, relations (16) and (17) are nothing but the Euler–Lagrange relations for the following minimum problem:

$$\min_{\boldsymbol{e}_*^{\mathrm{tr}}, \boldsymbol{q}_*} \left\{ \overline{D}(\boldsymbol{e}_*^{\mathrm{tr}} - \boldsymbol{e}_n^{\mathrm{tr}}, \boldsymbol{q}_* - \boldsymbol{q}_n) + \overline{\Psi}(\theta, \boldsymbol{e}, \eta, \boldsymbol{e}_*^{\mathrm{tr}}, \boldsymbol{q}_*) \right\} \tag{18}$$

along with positions $(16)_1$–$(16)_3$. In the latter, the regularized dissipation

$$\overline{D}(\boldsymbol{e}^{\mathrm{tr}}, \boldsymbol{q}) = \sup_{\overline{F}(\boldsymbol{A},\boldsymbol{B}) \leqslant 0} \{\boldsymbol{A} : \boldsymbol{e}^{\mathrm{tr}} + \boldsymbol{B} : \boldsymbol{q}\}$$

is defined as the Fenchel–Legendre conjugate of the indicator function of the regularized non-empty, convex, and closed domain

$$\overline{\mathscr{E}} = \{(\boldsymbol{A}, \boldsymbol{B}) : \overline{F}(\boldsymbol{A}, \boldsymbol{B}) \leqslant 0\}.$$

The minimum problem (18) corresponds in this setting to the Euler method where, nevertheless, the usual incremental quotients are replaced by the weaker distance $\overline{D}(\boldsymbol{e}_*^{\mathrm{tr}} - \boldsymbol{e}_n^{\mathrm{tr}}, \boldsymbol{q}_* - \boldsymbol{q}_n)$.

It is beyond the purposes of this paper to provide mathematical results on the above introduced minimum problem (18). Following Mielke (in press) and the upcoming contribution by Auricchio et al. (in preparation-a), we however stress that problem (18) is uniquely solvable and that the incremental solutions arising from the step-by-step solution of the minimization problem converge to a time-continuous solution of the constitutive relation as the diameter of the time partition I goes to zero. Moreover, the model is stable with respect to the regularization parameter $\delta > 0$. In particular, solutions to the incremental problem (18) converge to the unique minimizer of problem

$$\min_{\boldsymbol{e}_*^{\mathrm{tr}}, \boldsymbol{q}_*} \left\{ D(\boldsymbol{e}_*^{\mathrm{tr}} - \boldsymbol{e}_n^{\mathrm{tr}}, \boldsymbol{q}_* - \boldsymbol{q}_n) + \Psi(\theta, \boldsymbol{e}, \eta, \boldsymbol{e}_*^{\mathrm{tr}}, \boldsymbol{q}_*) \right\}, \tag{19}$$

as δ goes to zero.

4. Numerical results

To show the model capability of reproducing the macroscopic behaviour of SMA materials, we perform a number of stress-driven numerical experiments. In all tests we consider the material properties specified in Table 1 and compatible with Cu-based alloys (see, e.g., Šittner et al., 1995; Šittner and Novák, 2000), where E and ν are, respectively, the Young's modulus and the Poisson's ratio, while all the other material constants have already been introduced in Section 2.

The investigated problems are of the following types:

- uniaxial tests,
- biaxial tests,
- combined uniaxial tests.

Uniaxial tests represent the simplest setting on which it is possible to show the main features of the model as well as to appreciate the role played by the single material parameters, while biaxial tests allow to assess the model behaviour under complex non-proportional multi-axial loading conditions. Finally, combined uniaxial tests consist of uniaxial

Table 1
Material parameters

Parameter	Value	Unit
E	5×10^4	MPa
ν	0.35	–
β	2	MPa K^{-1}
M_f	223	K
h	1000	MPa
R	50	MPa
ε_L	4	%
δ	10^{-8}	–

loops in one direction followed by uniaxial loops in an orthogonal direction and they are suited for studying the model response under a sudden loading direction change. All the numerical experiments have been performed in both the pseudo-elastic and the shape-memory regimes, but for brevity we report here only the most significative examples.

4.1. Uniaxial tests

To begin with, we consider the following uniaxial tests in the pseudo-elastic regime:

- single and multiple tension cycles with permanent inelasticity,
- multiple tension cycles followed by multiple compression cycles with saturating permanent inelasticity,
- multiple tension cycles with saturating permanent inelasticity, including degradation effect.

On the other hand, in the shape-memory regime, we consider

- multiple tension cycles at $T = M_f$, each one followed by heating strain recovery.

For each experiment, we plot the output axial stress–axial strain curve. Moreover, for the tests consisting of single and multiple tension cycles with permanent inelasticity, we report also the output histories for the axial components of the internal variables (e^{tr}_{11} and q_{11}) and for the associated stress norms ($\|\boldsymbol{X}\|$ and $\|\boldsymbol{Q}\|$).

- Single and multiple tension cycles with permanent inelasticity.
  The first considered uniaxial test consists of studying the response of the model under tension cycles reaching a maximum axial stress of $\sigma_{max} = 300$ MPa. The numerical experiments are performed at a temperature $T = 298$ K and using the following model parameters: $H = 0$ MPa, $A = 0$ MPa and $\kappa = 2\%$. The choice of a non-zero parameter κ gives rise to a permanent inelasticity phenomenon. The left part of Fig. 4 and Fig. 5

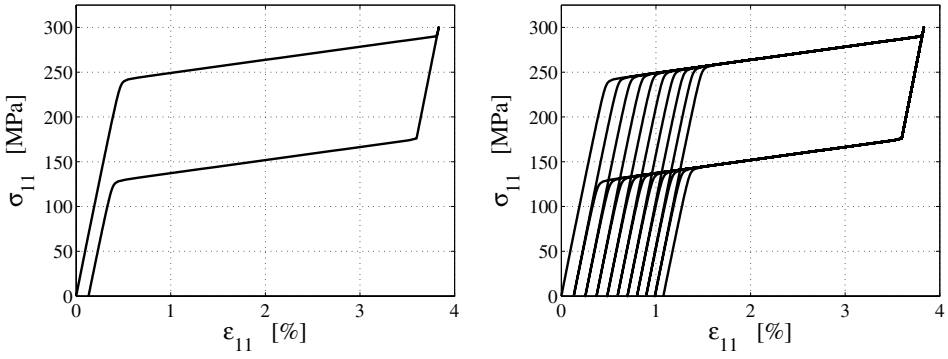

Fig. 4. Uniaxial tests: tension cycles with permanent inelasticity ($H = 0$ MPa, $A = 0$ MPa, $\kappa = 2\%$, $T = 298$ K). Axial stress–axial strain output for single (left) and multiple (right) tension loops.

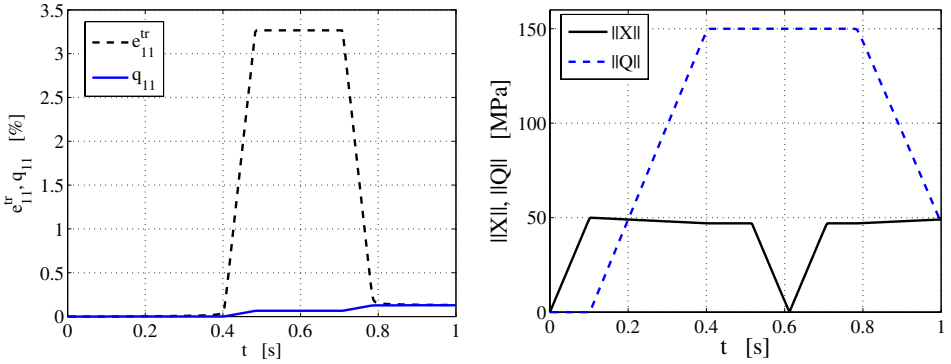

Fig. 5. Uniaxial tests: single tension cycle with permanent inelasticity ($H = 0$ MPa, $A = 0$ MPa, $\kappa = 2\%$, $T = 298$ K). Output histories for e_{11}^{tr} and q_{11} (left) and $\|\boldsymbol{X}\|$ and $\|\boldsymbol{Q}\|$ (right).

refer to a single tension cycle, while the right part of Fig. 4 and Fig. 6 refer to ten tension cycles. It is possible to observe the significant evolution of q_{11}, which represents the level of transformation strain that is not recovered during the unloading phase to $\sigma_{11} = 0$.

- Multiple tension cycles followed by multiple compression cycles with saturating permanent inelasticity.
  The goal of this test is to show the saturation of the permanent inelasticity (see Observation 6 of Section 2). The experiment is performed at a temperature $T = 298$ K and using the following model parameters: $H = 1.5 \times 10^4$ MPa, $A = 0$ MPa and $\kappa = 2\%$. The left part of Fig. 7 shows the response to ten tension cycles. We note that, since H is different from zero, the permanent strain saturates and does not exceed the threshold

$$\sqrt{2/3}\beta\langle T - M_{\mathrm{f}}\rangle/H = \sqrt{2/3} \times 150/(1.5 \times 10^4) = 0.816\%.$$

  The right part of Fig. 7 reports the results when fifteen compression cycles follow the tension ones. Again, we can observe that permanent inelasticity is accumulated and saturates when reaching the same threshold as in the case of tension.

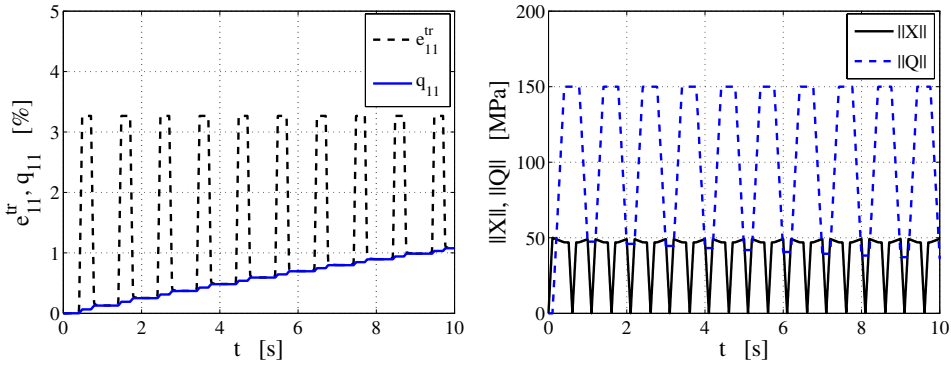

Fig. 6. Uniaxial tests: 10 tension cycles with permanent inelasticity ($H = 0$ MPa, $A = 0$ MPa, $\kappa = 2\%$, $T = 298$ K). Output histories for e_{11}^{tr} and q_{11} (left) and $\|\boldsymbol{X}\|$ and $\|\boldsymbol{Q}\|$ (right).

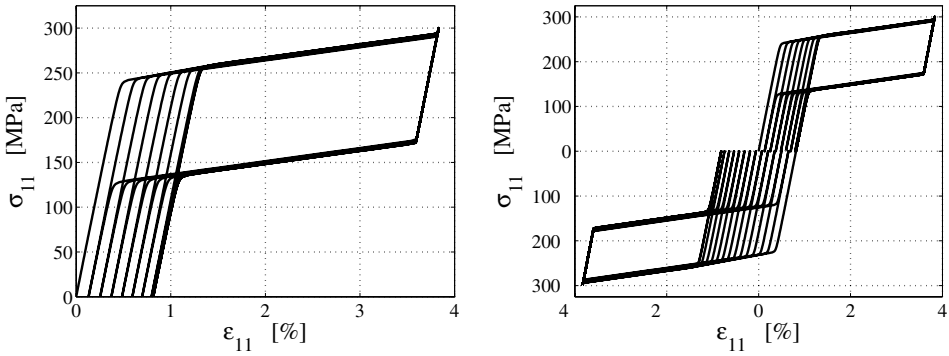

Fig. 7. Uniaxial tests: 10 tension cycles (left) and 10 tension followed by 15 compression cycles (right) with saturating permanent inelasticity ($H = 1.5 \times 10^4$ MPa, $A = 0$ MPa, $\kappa = 2\%$, $T = 298$ K). Axial stress–axial strain output.

- Multiple tension cycles with saturating permanent inelasticity, including degradation effect.
  We now want to investigate the effect induced on the model by the parameter A coupling the two internal variables. The experiment consists of fifteen tension loops performed at a temperature $T = 298$ K and using the following model parameters: $H = 1.5 \times 10^4$ MPa, $A = 2 \times 10^3$ MPa and $\kappa = 2\%$. As shown in Fig. 8, the choice of a non-zero value for A results in shifting down the loops. This sort of degradation effect is an important feature of the model as an analogous phenomenon is observed in experimental tests (see Fig. 1).
- Multiple tension cycles at $T = M_f$, each one followed by heating strain recovery.
  The aim of this last uniaxial experiment is to study the behaviour of the model when reproducing the shape-memory effect. The input consists of ten cycles, each one constructed as a tension loop with a maximum stress $\sigma_{max} = 150$ MPa at a temperature $T = M_f$ followed by a heating process at a constant zero stress up to a temperature of 298 K. The left part of Fig. 9 refers to a test with $H = 0$ MPa, $A = 0$ MPa and

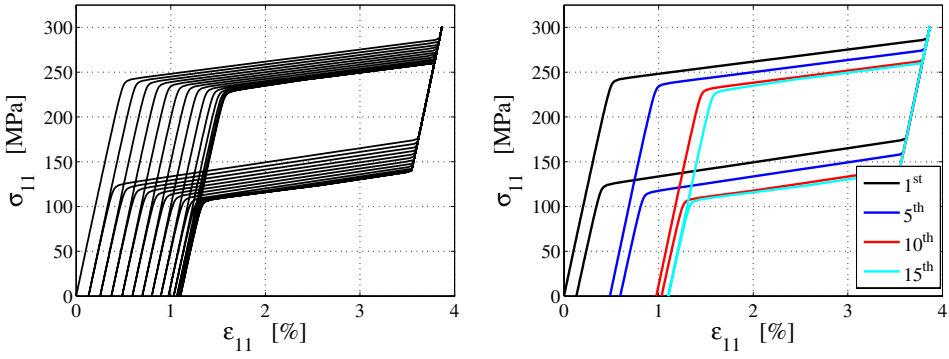

Fig. 8. Uniaxial tests: 15 tension cycles with saturating permanent inelasticity, including degradation effect ($H = 1.5 \times 10^4$ MPa, $A = 2 \times 10^3$ MPa, $\kappa = 2\%$, $T = 298$ K). Axial stress–axial strain output.

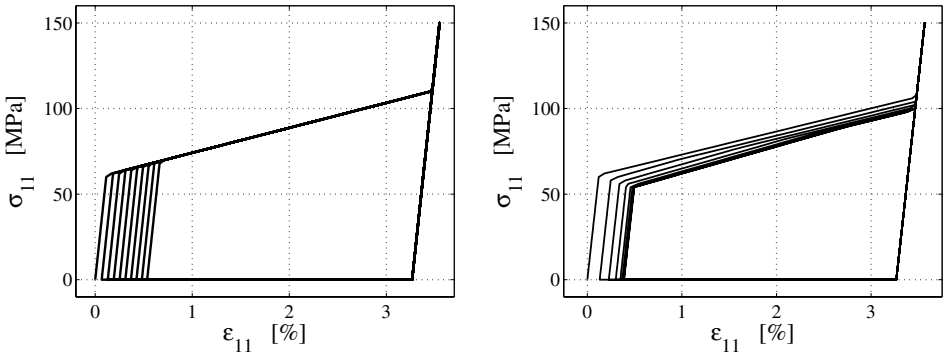

Fig. 9. Uniaxial tests: multiple (10) tension cycles at $T = M_f$, each one followed by heating strain recovery, with $H = 0$ MPa, $A = 0$ MPa (left) and $H = 1.5 \times 10^4$ MPa, $A = 2 \times 10^3$ MPa (right) and $\kappa = 2\%$. Axial stress–axial strain output.

$\kappa = 2\%$, while the right part refers to a test with $H = 1.5 \times 10^4$ MPa, $A = 2 \times 10^3$ MPa and $\kappa = 2\%$. Both of them show that an inelastic effect is activated, so that we observe only a partial shape recovery. We finally stress that in the first case, since $A = 0$ MPa, inelasticity is activated only during the heating process.

4.2. Biaxial tests

The goal of biaxial tests is to verify the behaviour of the model and its capability of reproducing permanent inelasticity when subjected to non-proportional multi-axial loading. Accordingly, we study the model response under the two following loading conditions:

- non-proportional hourglass-shaped test,
- non-proportional square-shaped test.

For both of these numerical experiments, we report the stress input and the corresponding strain output plots.

- Non-proportional hourglass-shaped test.
  The first considered biaxial test consists of a non-proportional test where σ_{11} and σ_{12} are led to $\sigma_{max} = 300$ MPa in the hourglass-shaped loading history of Fig. 10 (left), which is repeated five times. The experiment is performed at a temperature $T = 298$ K and using the following model parameters: $H = 1.5 \times 10^4$ MPa, $A = 4 \times 10^3$ MPa and $\kappa = 10\%$. The numerical results, reported in terms of first and fifth cycle in Fig. 10 (right), show that the new formulation proposed is capable of introducing and controlling permanent inelasticity effects even in non-proportional multi-axial tests.
- Non-proportional square-shaped test.
  The second biaxial test consists of a square-shaped loading history, repeated five times, where σ_{11} and σ_{22} are led to $\sigma_{max} = 300$ MPa as reported in Fig. 11 (left). The experiment

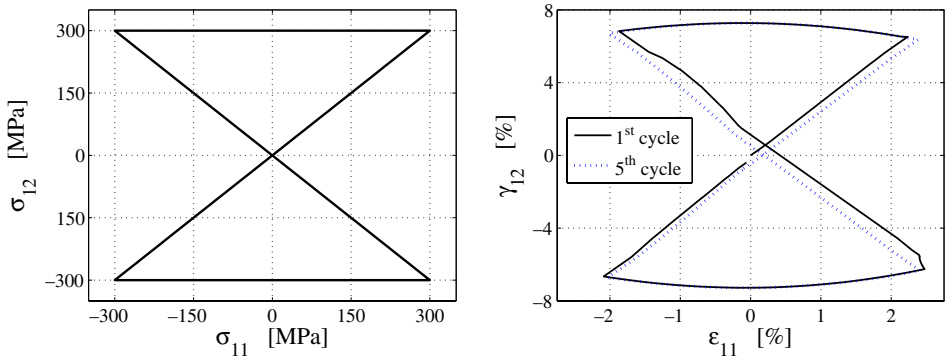

Fig. 10. Biaxial tests: non-proportional hourglass-shaped test ($H = 1.5 \times 10^4$ MPa, $A = 4 \times 10^3$ MPa, $\kappa = 10\%$, $T = 298$ K). $\sigma_{11} - \sigma_{12}$ input (left) and 1st and 5th cycle $\varepsilon_{11} - \gamma_{12}$ output (right).

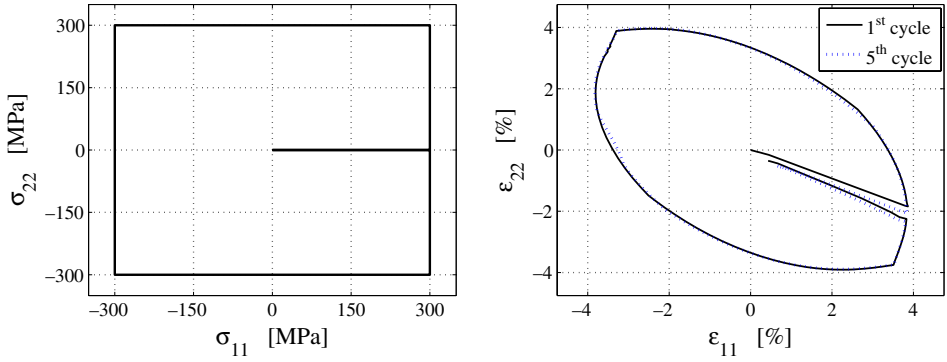

Fig. 11. Biaxial tests: non-proportional square-shaped test ($H = 1.5 \times 10^4$ MPa, $A = 4 \times 10^3$ MPa, $\kappa = 10\%$, $T = 298$ K). $\sigma_{11} - \sigma_{22}$ input (left) and 1st and 5th cycle $\varepsilon_{11} - \varepsilon_{22}$ output (right).

is performed at a temperature $T = 298$ K and using the following model parameters: $H = 1.5 \times 10^4$ MPa, $A = 4 \times 10^3$ MPa and $\kappa = 10\%$. The numerical results, shown in Fig. 11 (right), confirm the considerations from the previous test.

4.3. Combined uniaxial tests

The last numerical experiment shows the model response under loading conditions changing in their direction of application. It consists of uniaxial tension cycles whose direction is suddenly rotated of $\pi/2$.

- Ten tension cycles in direction 1 followed by 20 tension cycles in direction 2.
  This experiment is performed at a temperature $T = 298$ K and using the following model parameters: $H = 1.5 \times 10^4$ MPa, $A = 0$ MPa and $\kappa = 2\%$. Fig. 12 reports the stress input and the q_{11} and q_{22} output histories, while Fig. 13 shows the axial

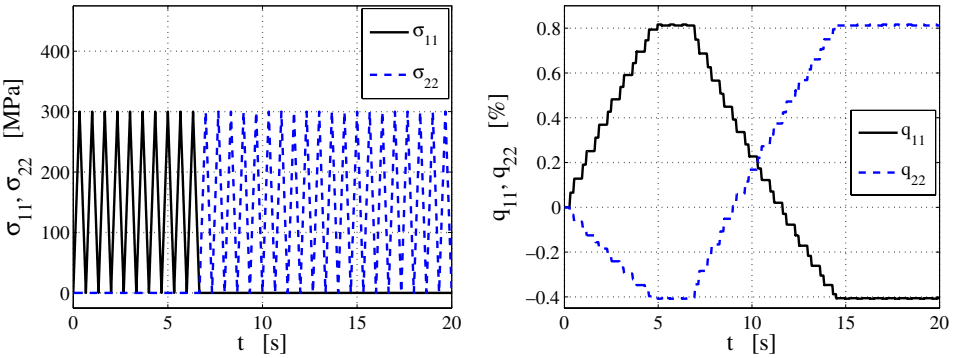

Fig. 12. Combined uniaxial tests: 10 tension cycles in direction 1 followed by 20 in direction 2 ($H = 1.5 \times 10^4$ MPa, $A = 0$ MPa, $\kappa = 2\%$, $T = 298$ K). Stress input histories (left) and q_{11} and q_{22} output histories (right).

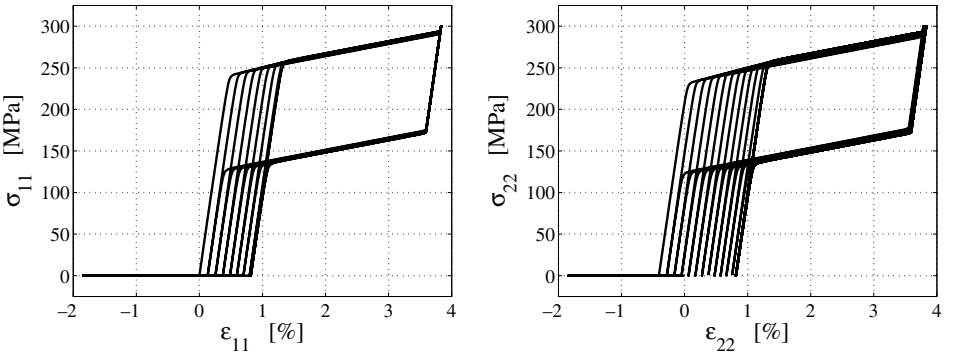

Fig. 13. Combined uniaxial tests: 10 tension cycles in direction 1 followed by 20 in direction 2 ($H = 1.5 \times 10^4$ MPa, $A = 0$ MPa, $\kappa = 2\%$, $T = 298$ K). $\sigma_{11} - \varepsilon_{11}$ output (left) and $\sigma_{22} - \varepsilon_{22}$ output (right).

stress–axial strain curves for the two loading directions. The numerical results prove the capability of the model of reproducing the features shown in uniaxial tests even under multi-axial loading conditions.

5. Conclusions

In the present paper, a new 3D constitutive model for describing the macroscopic behaviour of SMA has been proposed. With respect to the existing model considered as a starting point (i.e. Souza et al., 1998; Auricchio and Petrini, 2004a), this new one is able to describe SMA macroscopic behaviours taking into account also permanent inelasticity effects. Such effects can be introduced both with a saturating or a non-saturating evolution. Moreover, also degradation can be included. Many numerical experiments have been presented in order to show and assess the model performance both in uniaxial and non-proportional multi-axial problems. A generalization of the model (addressing for instance the different elastic behaviours in the austenitic and the martensitic phases), the

development of a detailed algorithmic strategy for solving the evolution equations governing the model, and its application to boundary value problems will be the subject of future communications.

Acknowledgements

This work has been partially developed within the joint French–Italian "Lagrange laboratory" project and has been partially supported by the Ministero dell'Istruzione, dell'Università e della Ricerca (MIUR) through the research program "Shape-memory alloys: constitutive modeling, structural analysis and design for innovative biomedical applications", as well as by the European Project HPRN-CT-2002-00284 "New Materials, Adaptive Systems and their Nonlinearities. Modelling, Control and Numerical Simulation".

References

Arrigoni, M., Auricchio, F., Cacciafesta, V., Petrini, L., Pietrabissa, R., 2001. Cyclic effects in shape-memory alloys: a one-dimensional continuum model. Journal de Physique IV France 11, 577–582.

Auricchio, F., Mielke, A., Stefanelli, U., in preparation. A rate-independent model for the evolution of shape memory materials.

Auricchio, F., Petrini, L., 2004a. A three-dimensional model describing stress-temperature induced solid phase transformations. Part I: solution algorithm and boundary value problems. International Journal for Numerical Methods in Engineering 61, 807–836.

Auricchio, F., Petrini, L., 2004b. A three-dimensional model describing stress-temperature induced solid phase transformations. Part II: thermomechanical coupling and hybrid composite applications. International Journal for Numerical Methods in Engineering 61, 716–737.

Auricchio, F., Reali, A., 2005. A one-dimensional model describing stress-induced solid phase transformation with residual plasticity. In: Proceedings of the II ECCOMAS Thematic Conference on Smart Structures and Materials, Lisbon.

Auricchio, F., Reali, A., Stefanelli, U., in preparation. Analysis of a model describing stress-induced solid phase transformation with permanent inelasticity.

Barlat, F., Aretz, H., Yoon, J.W., Karabin, M.E., Brem, J.C., Dick, R.E., 2005. Linear transformation-based anisotropic yield functions. International Journal of Plasticity 21, 1009–1039.

Bo, Z., Lagoudas, D.C., 1999. Thermomechanical modeling of polycrystalline SMAs under cyclic loading. Part III: evolution of plastic strains and two-way shape memory effect. International Journal of Engineering Science 37, 1175–1203.

Bouvet, C., Calloch, S., Lexcellent, C., 2004. A phenomenological model for pseudoelasticity of shape memory alloys under multiaxial proportional and nonproportional loadings. European Journal of Mechanics A/Solids 23, 37–61.

Brezis, H., 1973. Opérateurs maximaux monotones et semi-groupes de contractions dans les espaces de Hilbert. Number 5 in North-Holland Mathematics Studies. North-Holland, Amsterdam.

Clarke, F.H., 1990. Optimization and nonsmooth analysis, Classics in Applied Mathematics, second ed., vol. 5 Society for Industrial and Applied Mathematics (SIAM), Philadelphia, PA.

Duerig, T., Pelton, A., 2003. SMST-2003 Proceedings of the International Conference on Shape Memory and Superelastic Technology Conference, ASM International.

Duerig, T.W., Melton, K.N., Stoekel, D., Wayman, C.M., 1990. Engineering Aspects of Shape Memory Alloys. Butterworth-Heinemann, London.

Dutkiewicz, J., 1994. Plastic deformation of CuAlMn shape-memory alloys. Journal of Materials Science 29, 6249–6254.

Funakubo, H. (Ed.), 1987. Shape Memory Alloys. Gordon and Breach Science Publishers, New York (translated from the Japanese by J.B. Kennedy).

Govindjee, S., Kasper, E.P., 1997. A shape memory alloy model for uranium–niobium accounting for plasticity. Journal for Intelligent Material Systems and Structures 8, 815–823.

Govindjee, S., Miehe, C., 2001. A multi-variant martensitic phase transformation model: formulation and numerical implementation. Computer Methods in Applied Mechanics and Engineering 191, 215–238.

Helm, D., Haupt, P., 2003. Shape memory behaviour: modelling within continuum thermomechanics. International Journal of Solids and Structures 40, 827–849.

Lagoudas, D.C., Entchev, P., 2004. Modeling of transformation-induced plasticity and its effect on the behavior of porous shape memory alloys. Part I: constitutive model for fully dense SMAs. Mechanics of Materials 36, 865–892.

Leclercq, S., Lexcellent, C., 1996. A general macroscopic description of the thermomechanical behavior of shape memory alloys. Journal of Mechanics and Physics of Solids 44, 953–980.

Levitas, V.I., 1998. Thermomechanical theory of martensitic phase transformations in inelastic materials. International Journal of Solids and Structures 35, 889–940.

Levitas, V.I., Preston, D.L., 2002a. Three-dimensional Landau theory for multivariant stress-induced martensitic phase transformations. I. Austenite ↔ martensite. Physical Review B 66 (134206), 1–9.

Levitas, V.I., Preston, D.L., 2002b. Three-dimensional Landau theory for multivariant stress-induced martensitic phase transformations. II. Multivariant phase transformations and stress space analysis. Physical Review B 66 (134207), 1–15.

Mielke, A., in press. Evolution of rate-independent systems. In: Dafermos, C., Feireisl, E. (Eds.), Handbook of Differential Equations. Elsevier, Amsterdam.

Otsuka, K., Wayman, C.M. (Eds.), 1998. Shape Memory Materials. Cambridge University Press, Cambridge.

Paiva, A., Savi, M.A., Braga, A.M.B., Pacheco, P.M.C.L., 2005. A constitutive model for shape memory alloys considering tensile-compressive asymmetry and plasticity. International Journal of Solids and Structures 42, 3439–3457.

Peultier, B., Benzineb, T., Patoor, E., 2004. Modelling of the martensitic phase transformation for finite element computation. Journal de Physique IV France 115, 351–359.

Raniecki, B., Lexcellent, C., 1994. R_L models of pseudoelasticity and their specification for some shape-memory solids. European Journal of Mechanics, A: Solids 13, 21–50.

Simo, J.C., Hughes, T.J.R., 1998. Computational Inelasticity. Springer-Verlag, New York.

Šittner, P., Hara, Y., Tokuda, M., 1995. Experimental study on the thermoelastic martensitic transformation in shape memory alloy polycrystal induced by combined external forces. Metallurgical and Materials Transactions 26A, 2923–2935.

Šittner, P., Novák, V., 2000. Anisotropy of martensitic transformations in modeling of shape memory alloy polycrystals. International Journal of Plasticity 16, 1243–1268.

Souza, A.C., Mamiya, E.N., Zouain, N., 1998. Three-dimensional model for solids undergoing stress-induced phase transformations. European Journal of Mechanics, A: Solids 17, 789–806.

Vandermeer, R.A., Ogle, J.C., Northcutt Jr., W.G., 1981. A phenomenological study of the shape memory effect in polycrystalline uranium–niobium alloys. Metallurgical Transactions A 12A, 733–741.

Yeh, W.C., Lin, H.Y., 2006. An endochronic model of yield surface accounting for deformation induced anisotropy. International Journal of Plasticity 22, 16–38.